

Giant dipole resonance and shape evolution in Nd isotopes within TDHF method

A. Ait Ben Mennana¹, Y. EL Bassem¹, M. Oulne¹

¹ High Energy Physics and Astrophysics Laboratory, Department of Physics, Faculty of Sciences SEMLALIA, Cadi Ayyad University, P.O.B. 2390, Marrakesh, Morocco.

E-mail: oulne@uca.ma

December 2019

Abstract. The isovector giant dipole resonance (IVGDR) in even-even Nd isotopes from $A=124$ to $A=160$ is studied in the framework of time-dependent Hartree-Fock (TDHF) with Skyrme forces SkI3, SVbas, SLy5 and SLy6. The dipole strength is calculated and compared with the experimental data on photon absorption cross section σ_γ . An overall agreement between them is obtained. The dipole strengths in $^{124-140}\text{Nd}$ and $^{152-160}\text{Nd}$ are predicted. In addition, the correlation between the quadrupole deformation parameter β_2 and the splitting $\Delta E/\bar{E}_m$ of the giant dipole resonance (GDR) spectra is studied. The results confirm that $\Delta E/\bar{E}_m$ is proportional to β_2 . Shape phase transition in Nd isotopes is also investigated in the light of IVGDR.

1. Introduction

Giant resonances (GR) are an excellent example of collective modes in nuclei. Among different types of GRs, the most known and oldest is the isovector giant diople resonance (IVGDR). It was interpreted by Goldhaber and Teller (GT) as collective vibrations of the protons moving against the neutrons in the nucleus with the centroid energy of the form $E_c \propto A^{-1/6}$ [1]. On the other hand, Steinwedel and Jensen (SJ) interpreted it as a vibration of proton fluid against neutron fluid with a fixed surface where the centroid energy has the form $E_c \propto A^{-1/3}$ [2]. The experimental data are adjusted by a combination of these two [3]: in light nuclei, the data follow the law $A^{-1/6}$, while the dependence $A^{-1/3}$ becomes more and more dominant for increasing values of A . Also, it has been much studied from the experimental point of view (see for example Refs. [3–5]) as well as from the theoretical one (Refs. [6–9]).

Deformed nuclei provide an interesting testing ground since there is a strong interplay between the structure of the GDR and the ground-state deformation [10]. The isotopic chain of neodymium (Nd) between $A = 124$ and $A = 160$ belongs to a known region with a sudden transition from spherical to deformed shape in nuclei and vice versa, and is therefore an excellent field to investigate the effects of deformation in GDRs in

heavy deformed nuclei. GDRs in heavy deformed nuclei have been previously investigated by various microscopic methods such as time-dependent Skyrme-Hartree-Fock method [7, 11], Separable Random-Phase-Approximation (SRPA) [8, 12], Relativistic Quasiparticle Random Phase Approximation (RQRPA) [13] and Extended Quantum Molecular Dynamics (EQMD) [14]. The excitation of the GDRs in the experiment is induced by various ways, such as photoabsorption [4, 15] inelastic scattering [5, 16], γ -decay [17].

Many works based on the time-dependent Hartree-Fock (TDHF) approach have studied GRs in nuclei. The TDHF method provides a good approximation for GR. Early TDHF calculations concentrated on giant monopole resonance (GMR) [18, 19] because they require only a spherical one-dimensional code. In the last few years with the increase in computer power, large scale TDHF calculations become possible with no assumptions on the spatial symmetry of the system [7, 20, 21]. such calculations are performed by codes use a fully three dimensional (3D) Cartesian grid in coordinate space [22].

The isotopic chain of neodymium (Nd) has been studied in many previous works [7–9, 14] by different approaches. In Ref. [7], Maruhn et al. have studied the deformation dependence of giant dipole resonances (GDR) and its interplay with Landau fragmentation for some deformed heavy nuclei such as $^{142-150}\text{Nd}$ within TDHF by using two Skyrme forces SkI3 [23] and SLy6 [24]. They found that the results for these Nd isotopes are slightly downshift of order 1 MeV compared to experimental data [4]. In particular, the weakly deformed isotopes are dominated by Landau fragmentation which caused by coupling of the collective strength to 1ph states that are close in energy. In this work we extended this study to nineteen Nd isotopes by using different Skyrme forces.

The goal of the present work is to study the GDR and shape evolution in even-even Nd isotopes between $A=124$ and $A=160$ with TDHF theory [25] using SKY3D code [22], based on the Skyrme functional. This code uses a fully three dimensional (3D) Cartesian grid in coordinate space with no spatial symmetry restrictions and include all time-odd terms. Consequently, it is possible to study both spherical and deformed system within the limitation of mean field theory. Due to the open-shell nature of these nuclei, pairing and deformation properties must be taken into account in this study. Firstly, a static calculation gives some properties of the ground-state of nuclei like β_2 , γ . In dynamic calculation, the ground-state of nuclei is boosted by imposing a dipole excitation to obtain the GDR spectra and some of their properties (resonance energies, width).

The paper is outlined as follows: in Sec.2, we give a brief description of TDHF method and the GDR in deformed nuclei. In Sec.3, we present details of the numerical calculations. Our results and discussion are presented in Sec.4. Finally, Sec.5 gives the

summary.

2. The Time-Dependent Hartree-Fock method to giant resonances

2.1. The TDHF method

The TDHF is a self-consistent mean field (SCMF) theory which was proposed by Dirac in 1930 [26]. It generalizes the static hartree-Fock(HF) to dynamics problems to treat for example, the vibration of nuclei such as giant resonances [7, 18, 21, 27] and Heavy-ion collisions [20, 28]. Detailed discussions of TDHF theory can be found in several references [29–31]. The TDHF equations are obtained from the variation of Dirac action

$$S \equiv S_{t_0, t_1}[\psi] = \int_{t_0}^{t_1} dt \langle \psi(t) | \left(i\hbar \frac{d}{dt} - \hat{H} \right) | \psi(t) \rangle, \quad (1)$$

where $|\psi\rangle$ is the Slater determinant, t_0 and t_1 define the time interval, where the action S is stationary between the fixed endpoints t_0 and t_1 , and \hat{H} is the Hamiltonian of the system. The energy of the system is defined as $E = \langle \psi | \hat{H} | \psi \rangle$, and we have

$$\langle \psi | \frac{d}{dt} | \psi \rangle = \sum_{i=1}^N \langle \varphi_i | \frac{d}{dt} | \varphi_i \rangle, \quad (2)$$

where $|\varphi_i\rangle$ are the occupied single-particle states. The action S can be expressed as

$$\begin{aligned} S &= \int_{t_0}^{t_1} dt \left(i\hbar \sum_{i=1}^N \langle \varphi_i | \frac{d}{dt} | \varphi_i \rangle - E[\varphi_i] \right) \\ &= \int_{t_0}^{t_1} dt \left(i\hbar \sum_{i=1}^N \int dx \varphi_i^*(x, t) \frac{d}{dt} \varphi_i(x, t) - E[\varphi_i] \right) \end{aligned} \quad (3)$$

The variation of the action S with respect to the wave functions φ_i^* reads

$$\frac{\delta S}{\delta \varphi_i^*(x, t)} = 0, \quad (4)$$

for each $i = 1, \dots, N$, $t_0 \leq t \leq t_1$ and for all x . More details can be found for example in Refs. [30, 32]. We finally get the TDHF equation

$$i\hbar \frac{\partial}{\partial t} \varphi_i(t) = \hat{h}[\rho(t)] \varphi_i(t) \quad \text{for } 1 \leq i \leq N. \quad (5)$$

where \hat{h} is the single-particle Hartree-Fock Hamiltonian.

The TDHF equations (5) are solved *iteratively* by a small time step Δt during which we assume that the Hamiltonian remains constant. To conserve the total energy E, it is necessary to apply a symmetric algorithm by time reversal, and therefore to estimate the Hamiltonian at time $t + \frac{\Delta t}{2}$ to evolve the system between time t and $t + \Delta t$ [33, 34]

$$|\varphi(t + \Delta t)\rangle \simeq e^{-i \frac{\Delta t}{\hbar} \hat{h}(t + \frac{\Delta t}{2})} |\varphi(t)\rangle. \quad (6)$$

2.2. Giant dipole resonance in deformed nuclei

The GDR in deformed axially symmetric nuclei splits into two components with energies $E_i \sim R_i^{-1} \sim A^{-1/3}$ [2] where R is the nuclear radius, and even three resonances in the case of asymmetric nuclei. This splitting has been observed experimentally [3–5] and treated theoretically by different models [7–9]. For a spherical nucleus, the GDR spectra present one peak i.e the oscillations along the three axes have the same frequency $E_x = E_y = E_z$. For the axially symmetric prolate nuclei, the GDR spectra present two peaks where the low-energy E_z corresponds to the oscillations along the major axis of symmetry and the high-energy $E_x = E_y$ corresponds to the oscillations along transverse minor axes of the nuclear ellipsoid, due to $E \sim R^{-1}$. For an oblate nucleus, it is the opposite situation to the prolate case.

Among the properties of the ground-state of nuclei, there are the deformation parameters β_2 and γ which give an idea on the shape of the nucleus. These deformation parameters are defined as follows [22]

$$\beta = \sqrt{a_0^2 + 2a_2^2} \quad , \quad \gamma = \text{atan}\left(\frac{\sqrt{2}a_2}{a_0}\right), \quad (7)$$

where $a_m = \frac{4\pi}{5} \frac{Q_{2m}}{AR^2}$ with $R = r_0 A^{1/3}$.

3. Details of Calculations

In our study of GDR in isotopes of Nd ($Z = 60$) from $A = 124$ to $A = 160$, we used a TDHF code Sky3D (v1.1) [22]. This code solves the static Hartree-Fock (HF) as well as the time-dependent Hartree-Fock (TDHF) equations for Skyrme interactions [35]. This study was performed with four Skyrme forces: SkI3 [23], SVbas [36], SLy6 [24], SLy5 [24]. These Skyrme forces are widely used for the ground state properties (binding energies, radii...) and dynamics (as giant resonances) of nuclei including deformed ones. In particular they provide a reasonable description of the GDR: SLy6 and SkI3 [7, 8], SVbas [36] and SLy5 [11]. In Table 1, we summarize the parameters of these Skyrme forces used in this study.

The calculation is done in two successive steps for a given nucleus:

- *Static calculations:*

To carry out a TDHF calculations, an initial state is required. This state is obtained by running SKY3D code [22] in static mode, which solves the static HF + BCS equations (8) in a three-dimensional Cartesian basis *iteratively* until we obtain a convergence, i.e when for example the sum of the single-particle energy fluctuations becomes less than a certain value determined at the beginning of the static calculation. In this work we take as a convergence value 10^{-5} which is sufficient for heavy nuclei [22].

$$\hat{h}\psi_i(x) = \epsilon_i\psi_i(x) \quad \text{for } i = 1, \dots, A, \quad (8)$$

where \hat{h} is the single-particle Hamiltonien, and ϵ_i is the single-particle energy of the state $\psi_i(x)$ with $x = (\vec{r}, \sigma, \tau)$.

Table 1: Parameters (t, x) of the Skyrme forces used in this study.

Parameters	SkI3	SVbas	SLy6	SLy5
t_0 (MeV.fm ³)	-1762.880	-1879.640	-2479.500	-2484.880
t_1 (MeV.fm ⁵)	462.180	313.749	-1762.880	483.130
t_2 (MeV.fm ⁵)	-227.090	112.676	-448.610	-549.400
t_3 (MeV.fm ^{3+3σ})	8106.200	12527.389	13673.000	13763.000
x_0	0.308	0.258	0.825	0.778
x_1	-1.172	-0.381	-0.465	-0.328
x_2	-1.090	-2.823	-1.000	-1.000
x_3	1.292	0.123	1.355	1.267
σ	0.250	0.300	0.166	0.166
W_0 (MeV.fm ⁵)	188.508	124.633	122.000	126.000

In the input data file of SK3YD we use 24 as the number of grid points in the three cartesian directions ($n_x = n_y = n_z = 24$) and 1 fm as spacing between grid points ($dx = dy = dz = 1$ fm). Pairing is treated in the static calculation.

- *Dynamic calculations:*

The ground-state wave function obtained by the static calculations is excited by an instantaneous initial dipole boost operator in order to put the nucleus in the dipole mode [7, 37, 38].

$$\varphi_\alpha^{(g.s)}(r) \longrightarrow \varphi_\alpha(r, t = 0) = \exp(ib\hat{D})\varphi_\alpha^{(g.s)}(r), \quad (9)$$

where $\varphi_\alpha^{(g.s)}(r)$ represents the ground-state of nucleus before the boost, b is the boost amplitude of the studied mode, and \hat{D} the associated operator. In our case, \hat{D} represents the isovector dipole operator defined as

$$\begin{aligned} \hat{D} &= \frac{NZ}{A} \left(\frac{1}{Z} \sum_{p=1}^Z \vec{z}_p - \frac{1}{N} \sum_{n=1}^N \vec{z}_n \right) \\ &= \frac{NZ}{A} \left(\vec{R}_Z - \vec{R}_N \right), \end{aligned} \quad (10)$$

where \vec{R}_Z (resp. \vec{R}_N) measures the proton (resp. neutron) average position on the z axis.

In order to obtain the spectral distribution of the isovector dipole strength, we apply a boost (9) with a small value of the amplitude b to stay in the linear regime of the excitation. For a long enough time, the dipole moment $\hat{D} = \langle \psi(t) | \hat{D} | \psi(t) \rangle$ is recorded along the dynamical evolution. Finally, the dipole strength $S_D(\omega)$ can be obtained by performing the Fourier transform $D(\omega)$ of the signal $\hat{D}(t)$, defined as [39]

$$S_D(\omega) = \sum_{\nu} \delta(E - E_{\nu}) |\langle \nu | \hat{D} | 0 \rangle|^2. \quad (11)$$

Some filtering is necessary to avoid artifacts in the spectra obtained by cutting the signal at a certain final time, in order to the signal vanishes at the end of the

simulation time. In practice we use windowing in the time domain by damping the signal $D(t)$ at the final time with $\cos(\frac{\pi t}{2T_{fin}})^n$ [22].

$$D(t) \longrightarrow D_{fil} = D(t) \cdot \cos\left(\frac{\pi t}{2T_{fin}}\right)^n, \quad (12)$$

where n represents the strength of filtering and T_{fin} is the final time of the simulation. More details can be founded in Refs. [22, 40].

In this work, all dynamic calculations were performed in a cubic space with $24 \times 24 \times 24 \text{ fm}^3$ according to the three directions (x, y, z) and a grid spacing of 1 fm. We chose $n_t = 5000$ as number of time steps to be run, and $dt = 0.2 \text{ fm}/c$ is the time step, so $T_f = 1000 \text{ fm}/c$ is the final time of simulation. Pairing is frozen in the dynamic calculation i.e, the BCS occupation numbers are frozen at their initial values during time evolution.

4. Results and Discussion

4.1. Relation between nuclear shape and deformation parameters

The chain of Nd isotopes studied in this work belongs to a region that knows a transition between spherical, where the number of neutrons is close to $N=82$, and prolate or oblate shape when N increases or decreases [4, 9, 14]. The deformation parameters β_2 and γ give an estimate of the nuclei shape [39, 41]. In Table 2, we summarize the results obtained for the quadrupole deformation parameter β_2 of $^{124-160}\text{Nd}$ isotopes with four Skyrme forces within TDHF method, including the available experimental data from Ref. [42] and the HFB calculations based on the D1S Gogny force [43] for comparison. The variation of β_2 as a function of neutrons number N is plotted in Fig. 1.

As it can be seen from Fig.1, the agreement between the two theoretical calculations: this work and HFB based on the D1S Gogny force [43] theory. On the other hand, our calculations are generally in agreement with experimental data [42], whose maximum deviation reaches the value $\simeq 0.090$ in the case of the spherical nucleus ^{142}Nd . The discrepancy between theory and experiment is due to that the experimental data are, in fact, a total variance of β_2 while theoretical value is an expectation one. Thus theoretical β_2 values are allowed to be generally a bit smaller [44]. We notice also that the minimum of β_2 corresponds to the magic number of neutrons $N = 82$ where the nucleus ^{142}Nd has a spherical shape ($\beta_2 \simeq 0$) for the two theoretical calculations, while it is slightly deformed with experimental data ($\beta_2 \simeq 0.091$).

The results obtained for the deformation parameter γ are shown in Table 3, compared with those of HFB based on the D1S_Gogny effective nucleon-nucleon interaction [43]. We notice that the results obtained are almost the same for the four Skyrme forces and the Gogny interaction. There is a disagreement in the case of ^{132}Nd nucleus, where the Skyrme forces SkI3, SVbas, SLy5 and SLy6 give $13.2^\circ \leq \gamma \leq 18.1^\circ$ which shows that this nucleus is weakly triaxial, whereas Gogny interaction gives $\gamma = 0.0^\circ$ that means this nucleus has a prolate shape. For the spherical nucleus ^{142}Nd

Table 2: The quadrupole deformation parameter β_2 calculated with SkI3, SVbas, SLy6, and SLy5 are compared with the experimental data are from Ref. [42], and data from Ref. [43].

Nuclei	SkI3	SVbas	SLy6	SLy5	Exp. [42]	HFB_Gogny. [43]
^{124}Nd	0.414	0.415	0.421	0.418	—	0.421
^{126}Nd	0.395	0.396	0.407	0.404	—	0.407
^{128}Nd	0.370	0.374	0.386	0.383	—	0.373
^{130}Nd	0.356	0.355	0.422	0.400	0.370	0.417
^{132}Nd	0.270	0.280	0.289	0.295	0.349	0.444
^{134}Nd	0.242	0.237	0.249	0.251	0.249	0.244
^{136}Nd	0.198	0.193	0.205	0.207	—	0.176
^{138}Nd	0.170	0.119	0.173	0.173	—	0.139
^{140}Nd	0.081	0.000	0.089	0.083	—	0.000
^{142}Nd	0.000	0.000	0.000	0.000	0.091	0.000
^{144}Nd	0.087	0.068	0.087	0.083	0.123	0.076
^{146}Nd	0.169	0.153	0.164	0.158	0.152	0.165
^{148}Nd	0.221	0.208	0.216	0.214	0.201	0.201
^{150}Nd	0.348	0.308	0.335	0.321	0.285	0.266
^{152}Nd	0.353	0.343	0.347	0.345	—	0.350
^{154}Nd	0.358	0.354	0.356	0.354	—	0.345
^{156}Nd	0.364	0.360	0.367	0.365	—	0.354
^{158}Nd	0.371	0.364	0.370	0.367	—	0.365
^{160}Nd	0.377	0.364	0.371	0.367	—	0.361

where $\beta_2 \simeq 0$, the triaxiality is undefined that is why γ takes different values.

According to the results of the couple (β_2, γ) , we can predict the shape of the nucleus. So for Nd isotopes below $N = 82$, the isotopic chains exhibit a transition from deformed to spherical shape, and for neutron number higher than $N = 82$, both the experimental and calculated results show that the prolate deformation increases gradually and then saturates at a value which closes to $\beta_2 \simeq 0.365$.

4.2. Variation of the dipole moment

Alongside the static calculation giving some properties of the ground-state of $^{124-160}\text{Nd}$ isotopes, the dynamic calculation with the SKY3D code [22] allow to study some dynamic properties of theses nuclei such as the dipole moment $D_m(t)$ which is defined by Eq. (10). Fig. 2 shows the time evolution of the dipole moment $D_m(t)$ of $^{142-160}\text{Nd}$ isotopes calculated with Skyrme force SLy6. We note that the collective motion of nucleons in GDR is done generally along two axes. The oscillation frequency ω_i is related to the nuclear radius R_i by $\omega_i \propto R_i^{-1}$ where $i \in \{x, y, z\}$. For $^{124-130}\text{Nd}$ and $^{144-160}\text{Nd}$ isotopes, the oscillation frequencies along the symmetry z-axis (the dashed

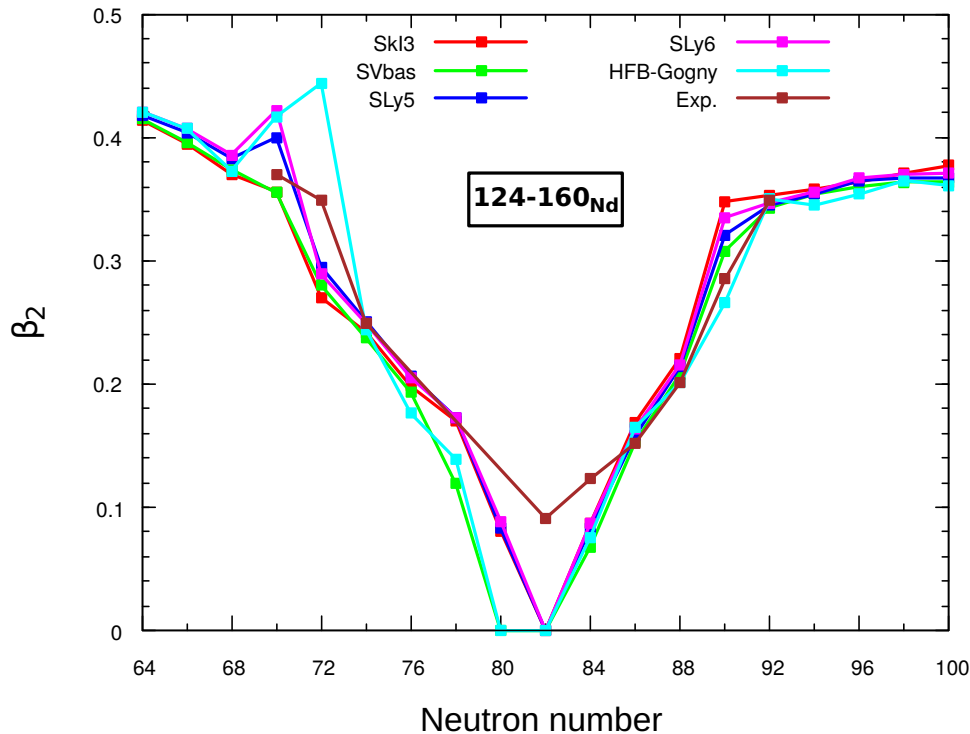


Figure 1: The Quadrupole deformation parameter β_2 of $^{124-160}\text{Nd}$ isotopes as function of their neutron number N . The experimental data are from Ref. [42].

line) are lower than that along the two other axes x and y (solid line) perpendicular to z -axis, which shows that these isotopes are deformed in prolate shape because $\omega_z < \omega_x = \omega_y$ [15]. That is why deformed nuclei have usually two splitting peaks in their GDR spectrum [3, 4]. For the nucleus ^{142}Nd , the oscillation frequencies along the three axes are equal ($\omega_x = \omega_y = \omega_z$), which show that it is spherical shape. We note also that the time evolution of dipole moment $D_m(t)$ is almost the same for the others Skyrme forces (SLy5, SkI3, SVbas).

Fig. 3 displays the time evolution of $D(t)$ for $^{132-138}\text{Nd}$ isotopes calculated with the Skyrme force SLy6. We notice that the oscillation frequencies ω_i along the three axes are different from each other $\omega_x \neq \omega_y \neq \omega_z$, which shows that these isotopes are weakly triaxial where $13.0^\circ \leq \gamma \leq 26^\circ$. We point out that $^{132-138}\text{Nd}$ is weakly triaxial with our calculation, but other works [45] found that it has prolate shape. Thus we tend to think that shape coexistence exist in this isotope.

4.3. GDR Spectrum

In order to obtain the energy spectrum of the GDR, we calculated the Fourier transform of the isovector signal $D(t)$. The spectral strength $S(E)$ (11) is simply the imaginary part of the Fourier transform of $D(t)$.

Table 3: The deformation parameters γ , calculated with SkI3, SVbas, SLy6, and SLy5 are compared with data from Ref. [43].

Nuclei	SkI3	SVbas	SLy6	SLy5	HFB_Gogny. [43]
^{124}Nd	0.0°	0.0°	0.0°	0.0°	0.0°
^{126}Nd	6.3°	0.0°	0.0°	0.0°	0.0°
^{128}Nd	0.0°	0.0°	0.0°	0.0°	0.0°
^{130}Nd	0.0°	0.0°	0.0°	0.0°	0.0°
^{132}Nd	18.1°	13.1°	15.9°	13.2°	0.0°
^{134}Nd	21.1°	21.7°	22.1°	22.0°	20.0°
^{136}Nd	21.5°	23.3°	23.0°	23.5°	21.0°
^{138}Nd	25.0°	0.1°	25.6°	25.9°	18.0°
^{140}Nd	0.1°	14.7°	0.0°	0.0°	0.0°
^{142}Nd	54.8°	39.5°	29.0°	29.2°	0.0°
^{144}Nd	0.2°	0.9°	0.1°	0.0°	0.0°
^{146}Nd	0.4°	0.0°	0.0°	0.0°	0.0°
^{148}Nd	0.0°	0.0°	0.0°	0.0°	0.0°
^{150}Nd	0.0°	0.0°	0.0°	0.0°	0.0°
^{152}Nd	0.0°	0.0°	0.0°	0.0°	0.0°
^{154}Nd	0.0°	0.0°	0.0°	0.0°	0.0°
^{156}Nd	0.0°	0.0°	0.0°	0.0°	0.0°
^{158}Nd	0.0°	0.0°	0.0°	0.0°	0.0°
^{160}Nd	0.0°	0.0°	0.0°	0.0°	0.0°

Figs. 4 - 6 show the GDR spectra in Nd isotopes computed with the four Skyrme forces, compared with the available experimental data [4]. It should be noted that the experimental GDR spectra for Nd isotopes from A=124 to A=140 and from A=152 to A=160 are not yet available, so we compared our results concerning these isotopes with those of SRPA theory [46] shown in Fig. 7. From Fig.4- 6, we can note that the deformation decreases gradually when the number of neutrons increases from N=64 (^{124}Nd) to number magic N=82 (^{142}Nd), and increases again until N=100 (^{160}Nd), which corresponds to a shape transition region of the Nd isotopes between deformed and spherical shape for N=82. We notice also that the resonance width Γ is related to deformation parameter β_2 as indicated on the right at the top of the panel in Figs. 4, 5, 6.

For all isotopes studied in this work except $^{132-138}\text{Nd}$ and ^{142}Nd , we notice that the oscillations along the major axis correspond to the lower centroid energy E_m^1 indicated by a dashed line in green, and along the minor axis correspond to the high energy E_m^2 indicated by a dotted-dashed line in blue, which shows that these nuclei are more or less deformed according to the values of the deformation parameters (β_2 , γ). For the nucleus ^{142}Nd which has a magic number N=82, the oscillations along the three axes correspond to the same resonance energy E_m , which means that ^{142}Nd has a spherical

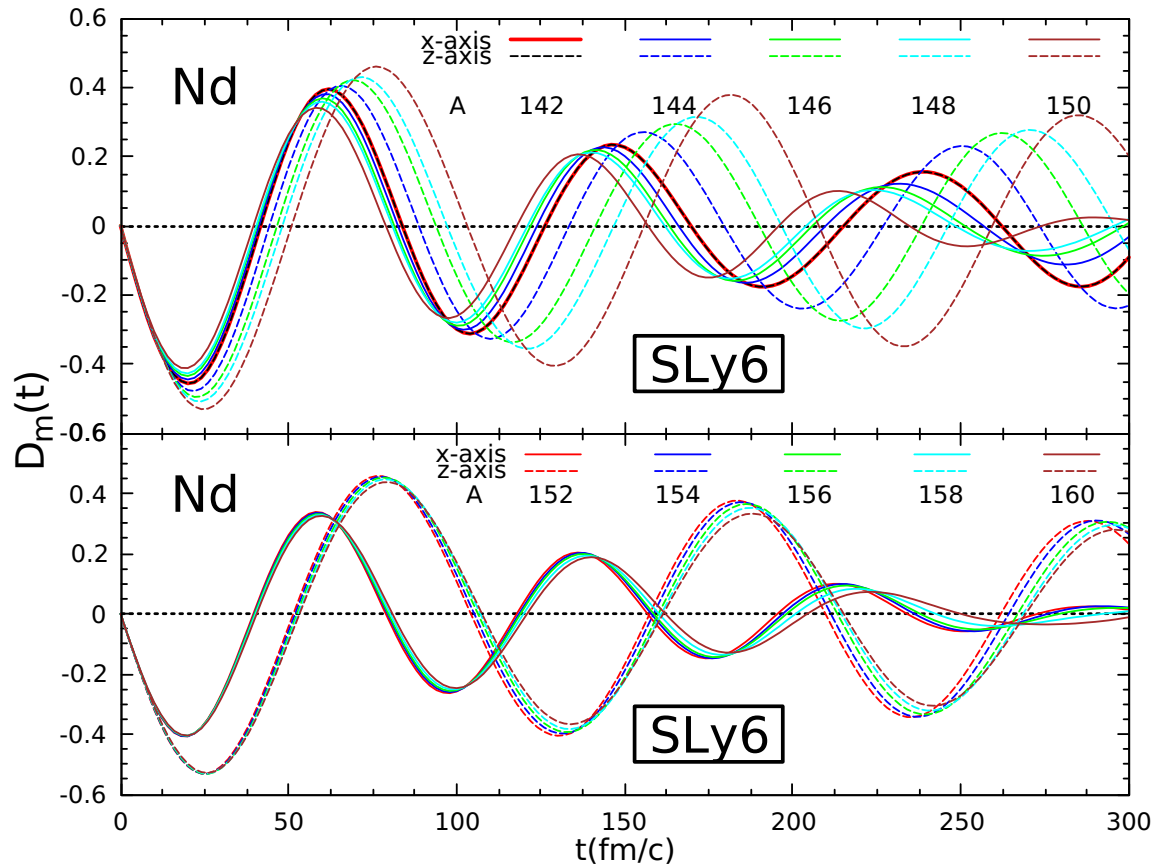


Figure 2: The dipole moment $D_m(t)$ as function of the simulation time $t(\text{fm}/c)$ calculated with the Skyrme force SLy6 using the SKY3D code [22] for Nd isotopes from $A=142$ to $A=160$.

shape.

For the isotopes ^{132}Nd , ^{134}Nd , ^{136}Nd and ^{138}Nd the oscillations along the three axes correspond to different energies $E_x \neq E_y \neq E_z$, so they have a degree of triaxiality. We point out that ^{138}Nd has prolate shape in case of Skyrme force SVbas where $\gamma = 0.1$, and is triaxial in case of the others Skyrme force (SLy6, SLy5, SkI3) where $\gamma \simeq 25$. Also for ^{140}Nd shown in Fig. 5, SVbas gives a spherical shape ($\beta_2=0$), while the others Skyrme forces predict weakly deformed ($\beta_2 \simeq 0.081$). The region with masse $\simeq 140$ is known by a variety of coexisting shape.

Fig. 5 compares the results of the GDR spectra for different Skyrme forces with the available experimental data [4]. It is seen that all four Skyrme forces provide in general acceptable agreement with the experimental data with a slight down-shift of the order of 0.5 MeV for SLy5, SLy6 and SkI3 in the case of the weakly deformed isotopes $^{142-148}\text{Nd}$, and slight up-shift (~ 0.5 MeV) for SVbas force. For spherical ^{142}Nd and weakly deformed ^{144}Nd and ^{146}Nd , the GDR spectrum is fragmented where appears a small shoulder due to the landau fragmentation. This fragmentation depends on the choice of the Skyrme force. For example, SVbas gives a weak fragmentation among the

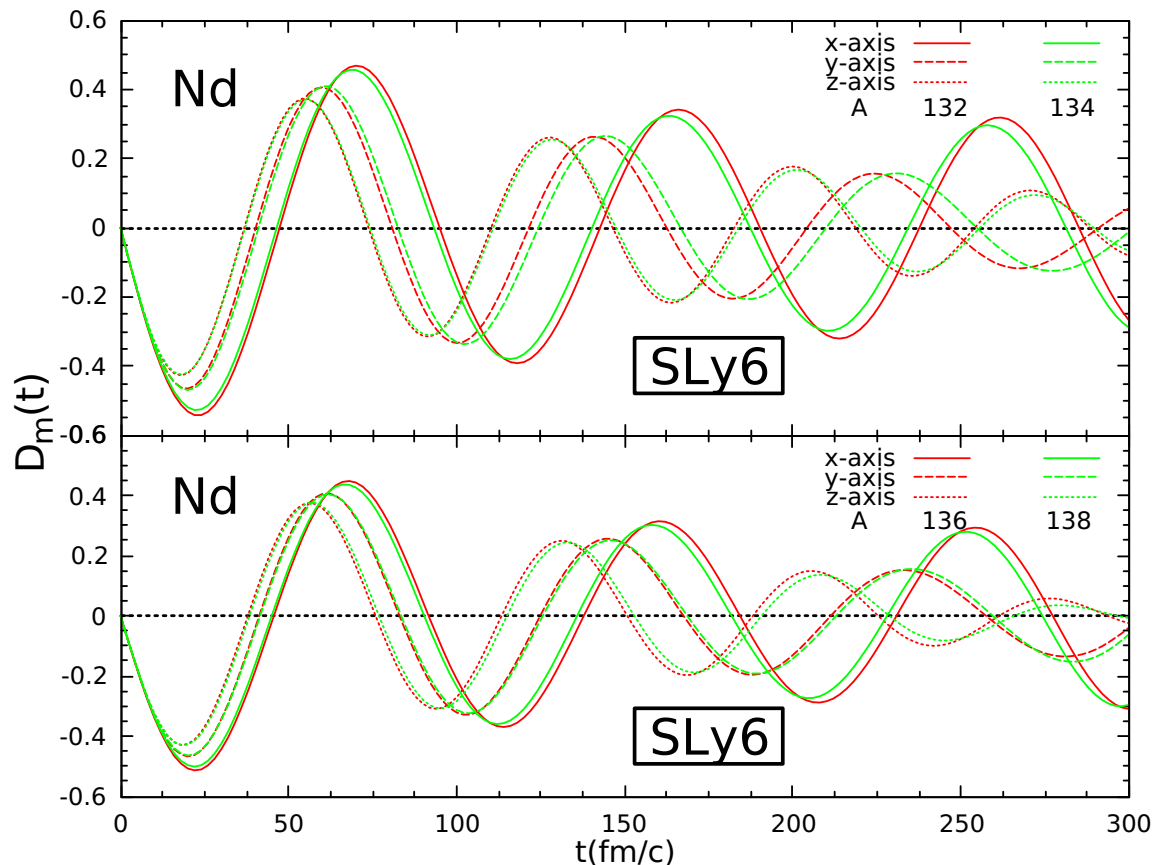


Figure 3: Same as in Fig. 2 for isotopes Nd from $A=132$ to $A=138$.

four forces of Skyrme. For ^{148}Nd , the small shoulder disappears in GDR spectrum only SkI3. The agreement is better for deformed isotope ^{150}Nd , where all Skyrme force produce the deformation splitting. In general, the force SVbas shows a further performance in respect to the other forces. We can see also, that Sly6 and Sly5 have good results with a slight advantage for Sly6.

In a previous work [46], such a problem has been studied with other different forces of ours, including SLy6. So, in Fig. 7, we compare our obtained results with SLy6 with those of that work [46]. From this figure, we can see an overall agreement between both calculations particularly for more deformed nuclei. We explain this mismatch of about 1 MeV: the results of two theoretical calculations (TDHF,SRPA) depend on their numerical realisations (size of configuration space, completeness of residual interaction, ...). SRPA was done in a limited space of 1ph configuration while TDHF includes effectively a much larger computational space. Larger is better and thus the TDHF results is more reliable. In Fig. 7, we compare also SRPA with SVBas results. Their results are very close to each other because SVbas produce a slightly higher peak position.

Fig. 8 shows a comparison of the strength GDR for the isotopes ^{124}Nd , ^{142}Nd , ^{150}Nd

and ^{160}Nd with the four Skyrme forces. We can see a small shift of the average peak position between these forces around ± 1 MeV. That means there is a dependence of the GDR spectra on Skyrme forces [12]. This dependence is related to some basic features and nuclear properties of the Skyrme functional as listed in Table 4. High sum rule enhancement factor $\kappa = (m_1^*/m)^{-1} - 1$ (i.e low isovector effective mass m_1^*/m) leads to a shift of the GDR strength towards the higher energy region as indicated in Ref. [36] in the case of GDR in ^{208}Pb and in Ref. [47] in the case of GDR in ^{174}Yb . For example, the large collective shift in SVbas can be related to a very high enhancement factor $\kappa=0.4$ compared to other Skyrme forces. For the deformed nucleus ^{150}Nd , we see that all these forces reproduce well the experimental data except for SkI3. The giant dipole resonance for SkI3 is lower than other forces because it has larger symmetry energy ($\sim 35\text{MeV}$) while 30-32 MeV is the standard value.

Table 4: The isovector effective mass m_1^*/m , sum rule enhancement factor $\kappa = (m_1^*/m)^{-1} - 1$, and symmetry energy a_{sym} for the Skyrme forces in this work [36], [24].

Forces	m_1^*/m	κ	$a_{sym}(\text{MeV})$
SLy6	0.80	0.25	31.96
SLy5	0.80	0.25	32.03
SkI3	0.80	0.246	34.80
SVbas	0.715	0.4	30.00

In order to compare our results obtained concerning the shape of Nd isotopes from GDR spectra with other theory, we perform a calculation of the total energy curves for $^{124-160}\text{Nd}$ with the covariant density functional theory (CDFT) [48–52] by using the very successful density-dependent meson-exchange relativistic energy functional DD-ME2 [50]. In Fig. 9 we display triaxial contour plots of $^{124-160}\text{Nd}$ isotopes in the $\beta\gamma$ -plane. To study the dependency on γ , a systematic constrained triaxial calculation has been done for mapping the quadrupole deformation space defined by β_2 and γ . The obtained energies are normalized with respect to the binding energy of the global minimum.

From Fig. 9, we can notice that, at the beginning of the chain, Nd isotopes have an axial prolate shape for $^{124-130}\text{Nd}$. Then, the location of the ground state minimum moves to triaxial shape at $^{132-138}\text{Nd}$. $^{140-144}\text{Nd}$ have a spherical shape, while the isotope ^{146}Nd appears as more deformed with a prolate shape. The ground state remains prolate up to the end of the isotopic chain (N=100). These results are in agreement with ours shown in Figs. 2 - 6 except for ^{132}Nd . The calculation with TDHF theory gives a weakly triaxial shape for ^{132}Nd as shown in Fig. 3, while a prolate shape is obtained with CDFT theory as shown in Fig. 9.

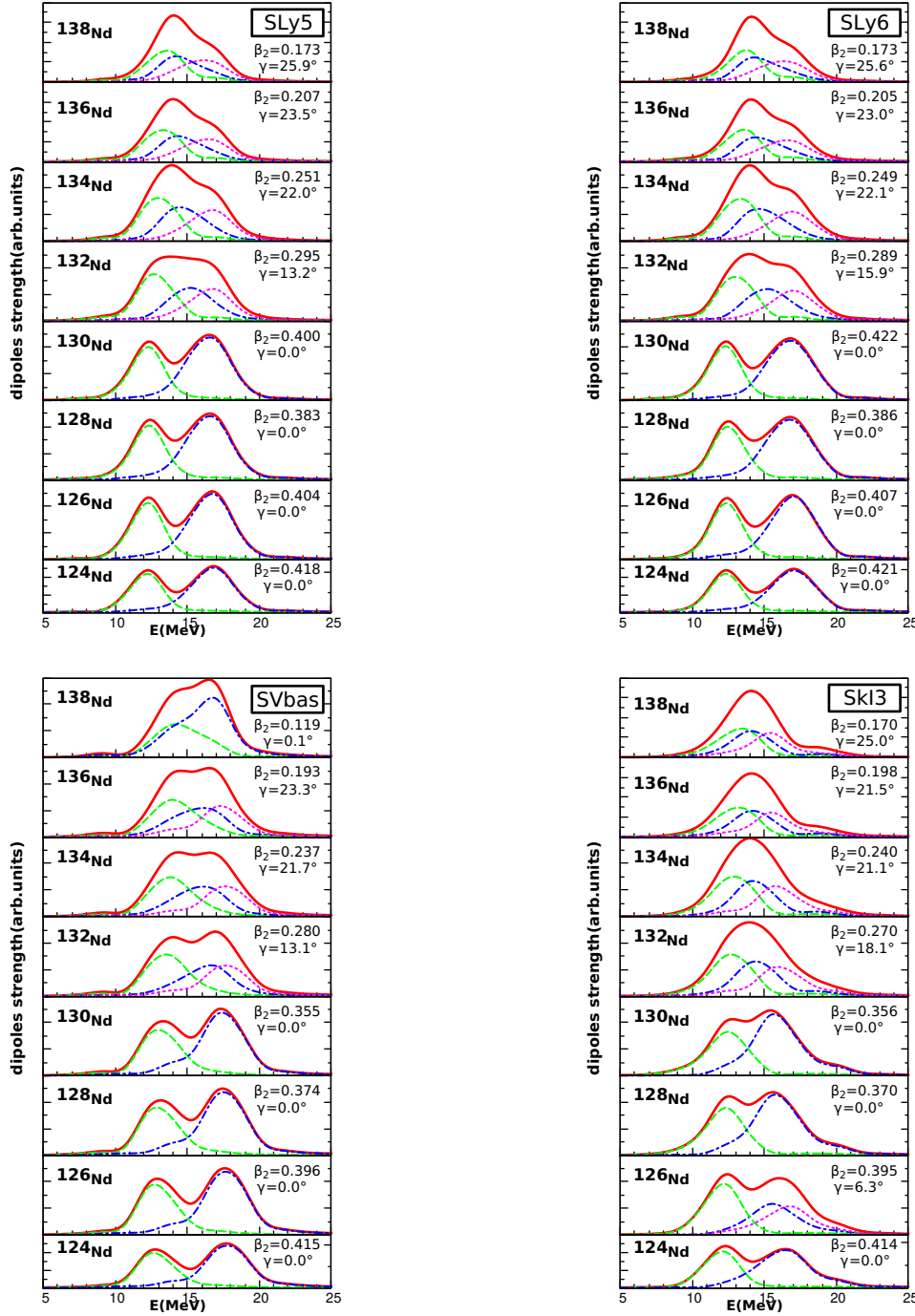


Figure 4: GDR spectra in the chain of $^{124-138}\text{Nd}$ calculated with SLy5, SLy6, SVbas and SkI3. The solid (red), dashed (green) and dotted-dashed (magenta) lines denote the dipole strengths: total, along the long axis and the short axis (multiplied by 2 except $^{132-138}\text{Nd}$) respectively. The dotted (brown) line denotes the strength along the third middle axis in the case of the triaxial nuclei $^{132-138}\text{Nd}$. The calculated strength total is compared with the experimental data [4] depicted by blue dots.

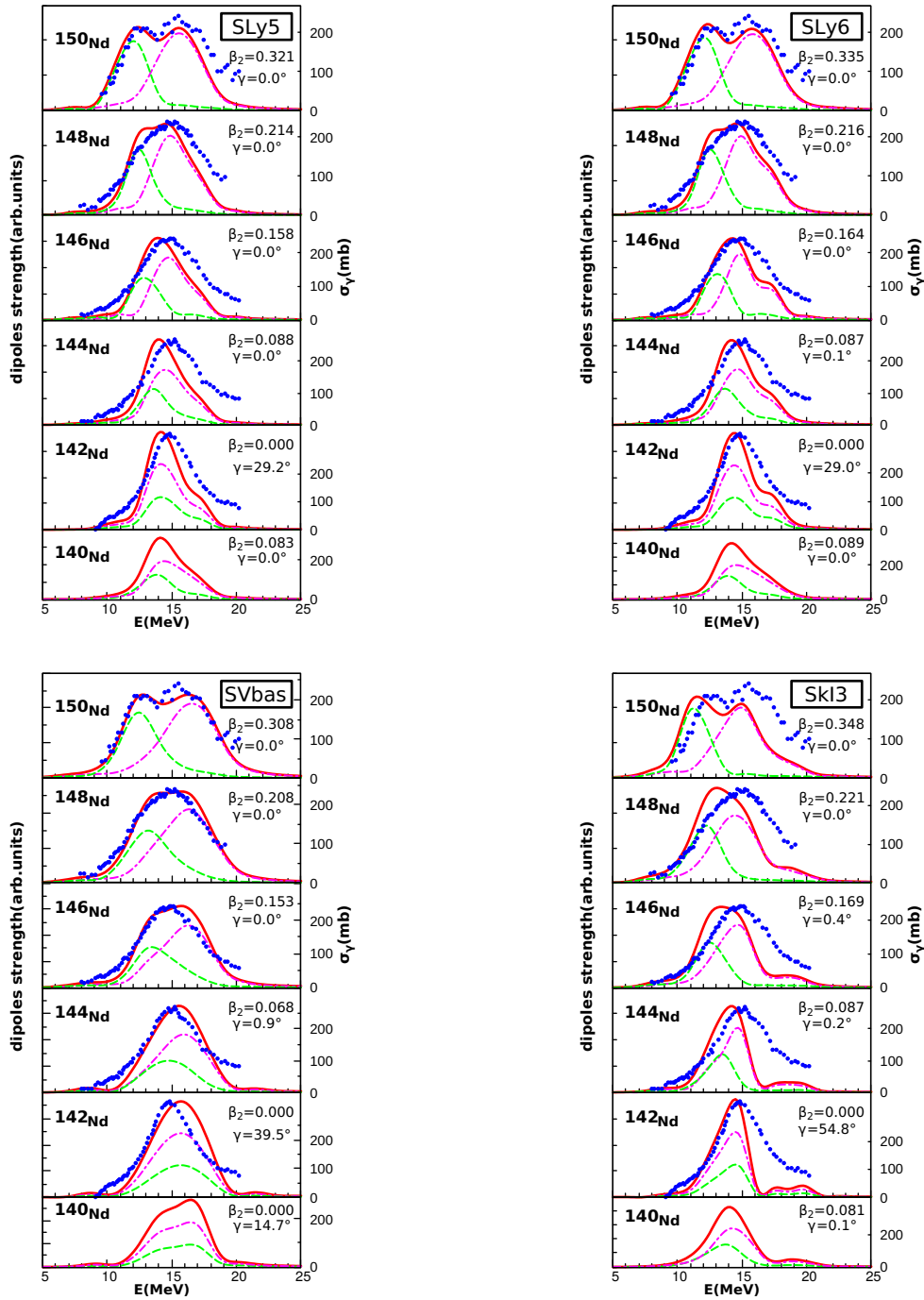


Figure 5: GDR spectra in the chain of $^{140-150}\text{Nd}$ calculated with SLy5, SLy6, SVbas and SkI3. The solid (red), dashed (green) and dotted-dashed (magenta) lines denote the dipole strengths: total, along the long axis and the short axis (multiplied by 2) respectively. The calculated strength total is compared with the experimental data [4] depicted by blue dots.

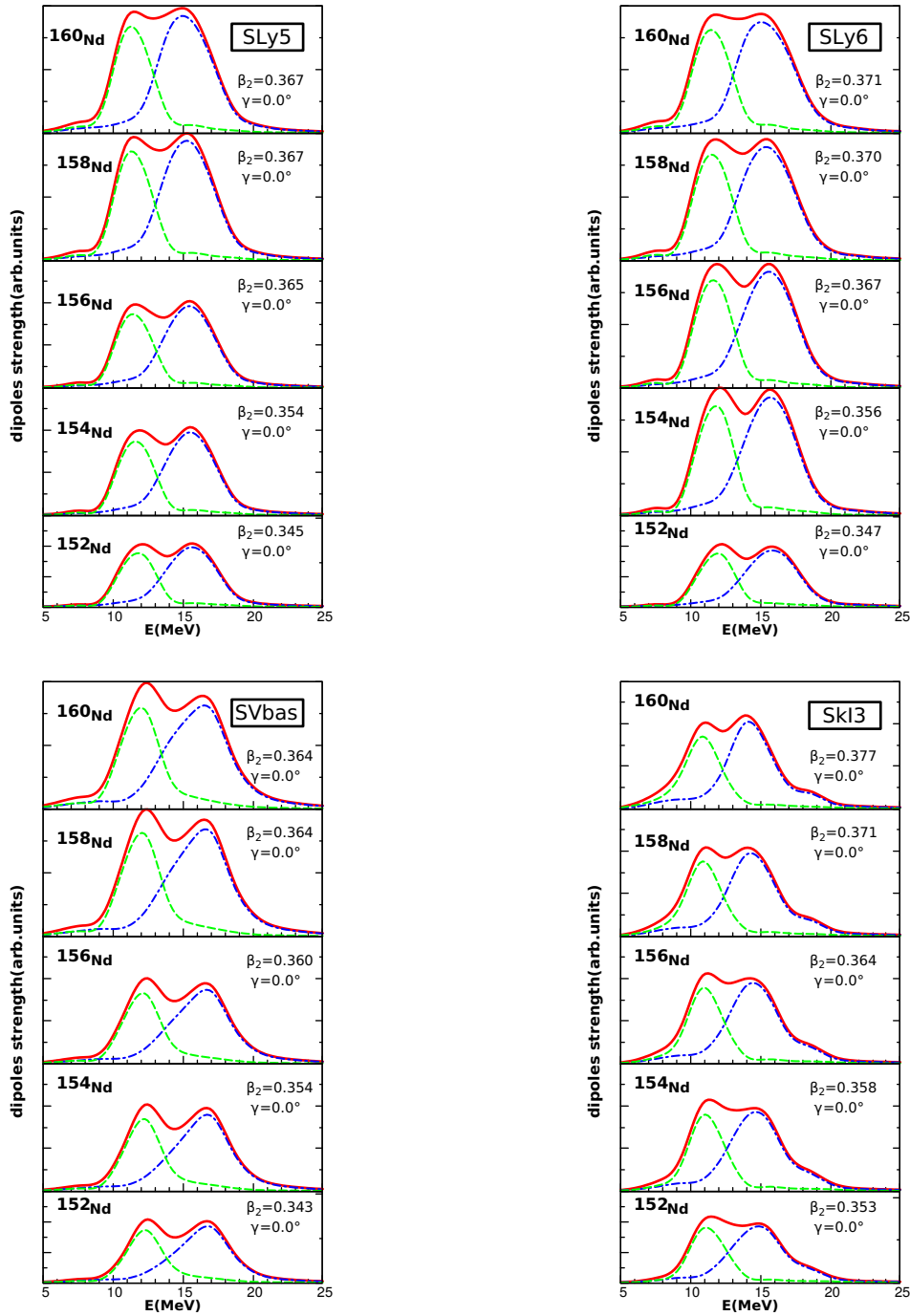


Figure 6: GDR spectra in the chain of $^{152-160}\text{Nd}$ calculated with SLy5, SLy6, SVbas and SkI3. The solid (red), dashed (green) and dotted-dashed (magenta) lines denote the dipole strengths: total, along the long axis and the short axis (multiplied by 2) respectively. The calculated strength total is compared with the experimental data [4] depicted by blue dots.

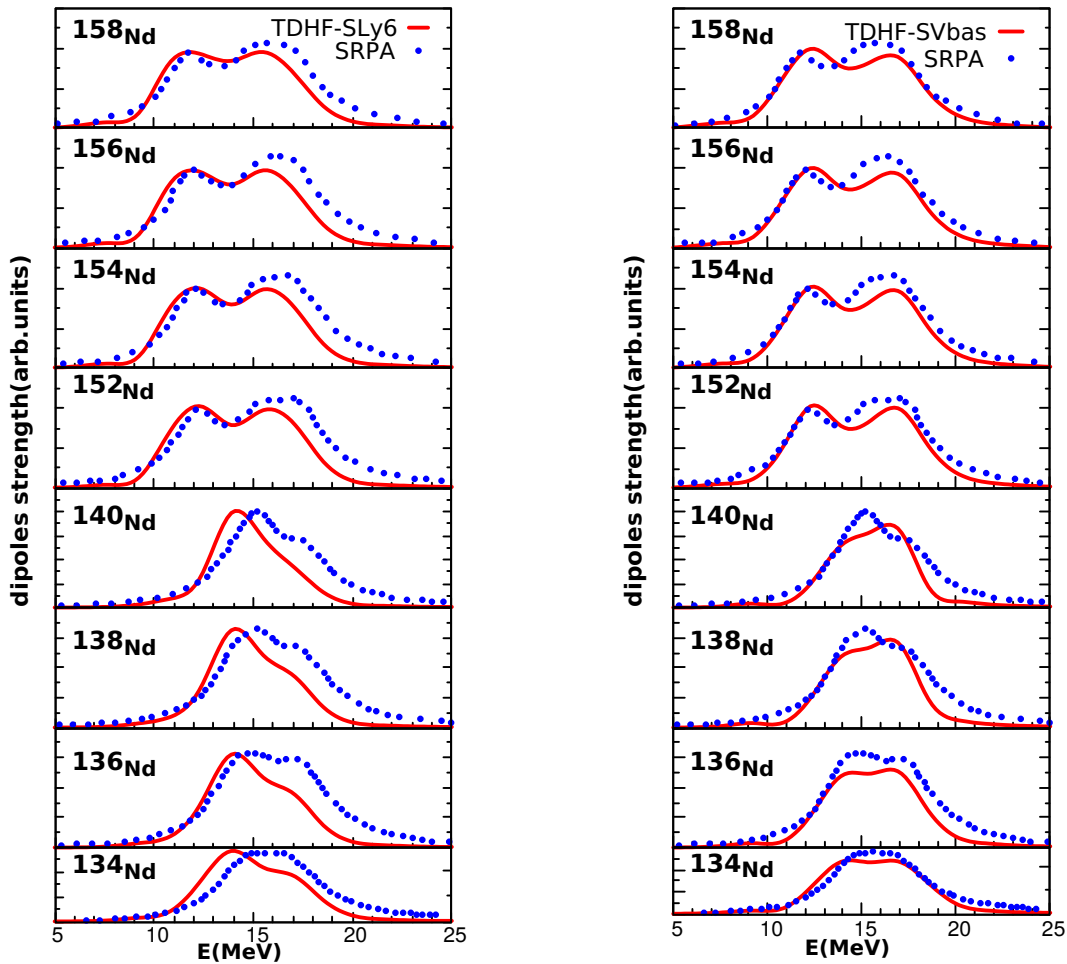


Figure 7: The GDR spectra in $^{134-140}\text{Nd}$ and $^{152-158}\text{Nd}$ calculated with the Skyrme forces SLy6 and SVbas (red line) are compared with SRPA theory [46] (blue dot).

4.4. Relation between deformation splitting ΔE and quadrupole deformation β_2

Among the properties of giant resonance, there is the resonance energy centroid defined by the formula

$$E_m = \frac{\int_0^{+\infty} S(E) E dE}{\int_0^{+\infty} S(E) dE}, \quad (13)$$

where $S(E)$ (11) is the strength function of GR. The total GDR spectrum generally presents two peaks for deformed nuclei, one corresponds to a resonance energy E_m^1 along the major axis and the other corresponds to a resonance energy E_m^2 along the minor axis. In Table 5, we summarize the TDHF calculation with the four Skyrme forces concerning E_m^1 and E_m^2 compared with the available experimental data from Ref. [4]. In Fig. 10, we plot E_m as function as number of neutrons. E_m^1 and E_m^2 denote the peak position of GDR along the minor axis and the major axis respectively. It is seen that the resonance energy E_m^1 along the minor axis decreases until $N=142$, and then trends to increase when the neutron number N increases. On the contrary, the resonance energy

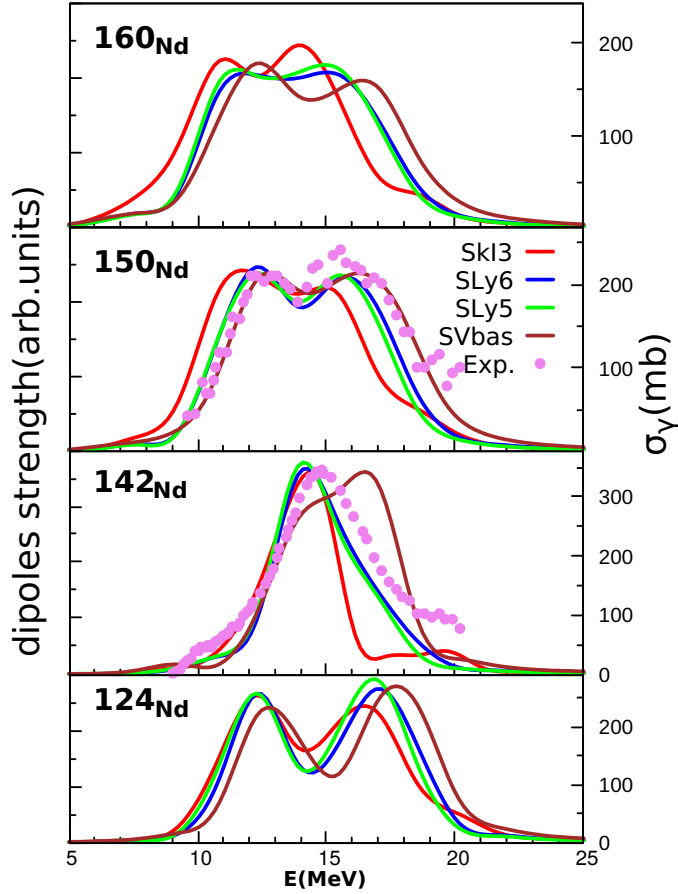


Figure 8: Comparison of calculated GDR spectra with Skyrme forces SkI3, SLy6, SLy5 and SVbas in case ^{124}Nd , ^{142}Nd , ^{150}Nd and ^{160}Nd . the experimental data [4] are depicted by purple dots.

E_m^2 along the major axis increases when N increases until $N=142$, and then gradually decreases. We note also, that the values of E_m^1 and E_m^2 calculated by these Skyrme forces are generally in agreement with the available experimental data with a small shift ± 0.5 MeV. The agreement is better for the Skyrme force SLy6, which was shown to be optimal for the description of the IVGDR in medium-heavy deformed nuclei [8].

In Fig. 11, the resonance energy E_m calculated with the four Skyrme forces is compared with the collective models Steinwedel-Jensen(SJ) [53]

$$E_{SJ} = 81.A^{-1/3} \text{MeV} \quad (14)$$

and Berman-Fultz (BF) [3]

$$E_{BF} = (31.2A^{-1/3} + 20.6A^{-1/6}) \text{MeV} \quad (15)$$

The latter treats dipole resonance as a combination of Steinwedel-Jensen($E_{SJ} \sim A^{-1/3}$) [53] and Goldhaber-Teller($E_{GT} \sim A^{-1/6}$) [1] models. It is seen that the calculated energies with SLy6 agree quite well with the BF estimate [3] until the $N=82$ shell closure,

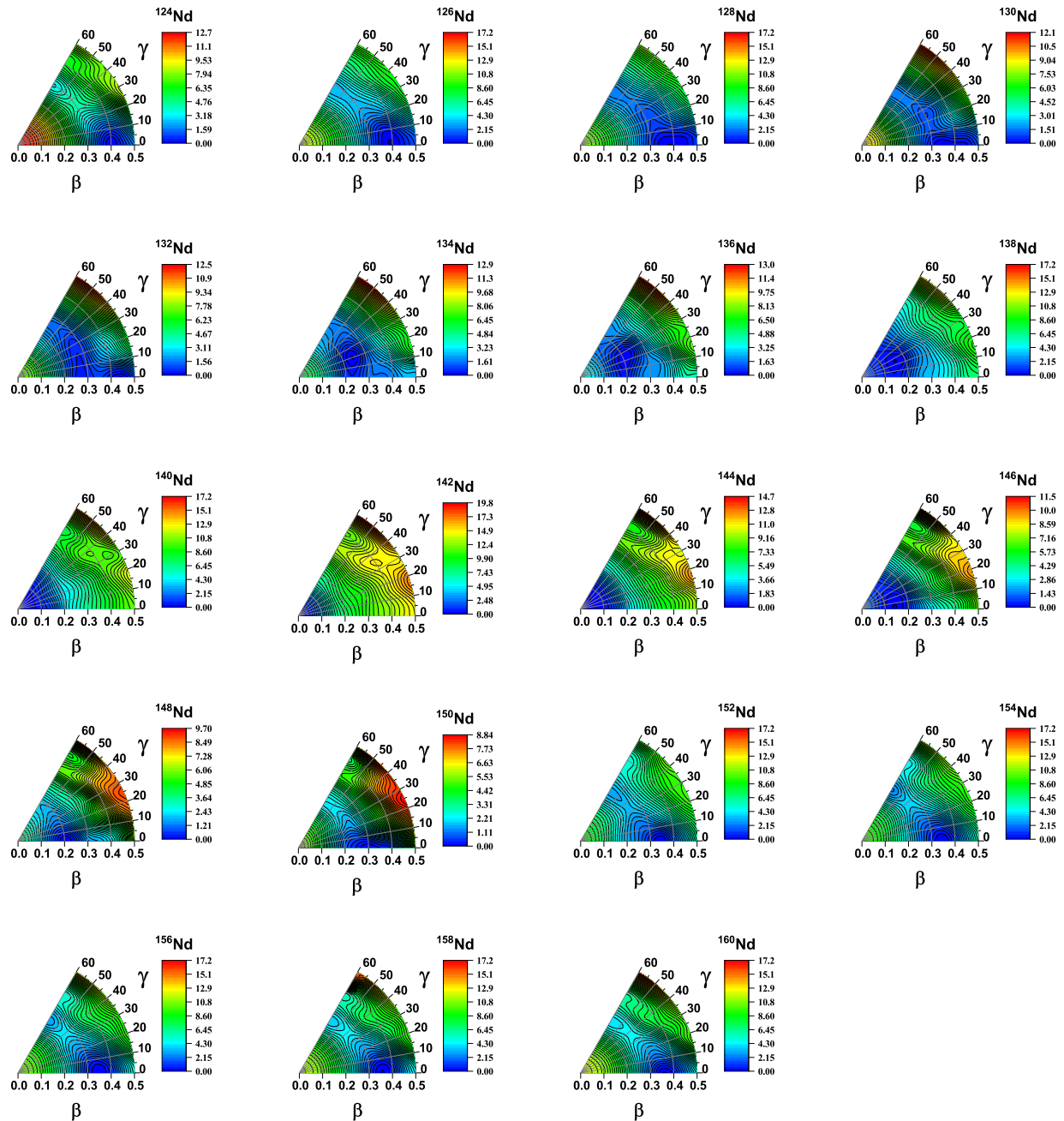


Figure 9: (Color online) The total energy curves for $^{124-160}\text{Nd}$ obtained within CDFT framework with DD-ME2 sets as a function of the axial quadrupole deformation parameter, β_2 .

while those calculated with SVbas are close to the SJ estimate [53]. But all Skyrme forces reproduce the overall trend of decreasing energy with increasing mass number A .

The deformation splitting ΔE is the difference between the resonance energy centroids along two axis $\Delta E = E_m^2 - E_m^1$. From Fig. 12, it can be easily seen for

Table 5: The resonance energy centroids E_m^1 and E_m^2 correspond respectively to oscillation along the major axis and the minor one. The experimental data are from ref. [4].

Nuclei	SkI3		SVBas		SLy5		SLy6		Exp. [4]	
	E_m^1	E_m^2	E_m^1	E_m^2	E_m^1	E_m^2	E_m^1	E_m^2	E_m^1	E_m^2
¹²⁴ Nd	12.48	16.75	13.34	18.00	12.52	16.86	12.71	17.17	—	—
¹²⁶ Nd	12.56	16.60	13.41	17.86	12.55	16.75	12.74	17.06	—	—
¹²⁸ Nd	12.62	16.36	13.51	17.70	13.63	16.59	12.81	16.88	—	—
¹³⁰ Nd	12.71	16.31	13.59	17.57	12.52	16.59	12.54	16.93	—	—
¹³² Nd	13.13	15.79	14.03	17.15	13.06	16.09	13.35	16.34	—	—
¹³⁴ Nd	13.28	15.63	14.31	16.90	13.35	15.88	13.59	16.13	—	—
¹³⁶ Nd	13.47	15.38	14.56	16.66	13.58	15.67	12.54	16.93	—	—
¹³⁸ Nd	13.64	15.22	14.92	16.31	13.79	15.52	13.35	16.34	—	—
¹⁴⁰ Nd	14.04	14.83	15.82	15.82	14.24	15.16	13.59	16.13	—	—
¹⁴² Nd	14.61	14.61	15.83	15.83	14.88	14.88	15.09	15.09	14.95± 0.10	—
¹⁴⁴ Nd	13.69	14.75	15.03	15.94	14.02	15.06	14.17	15.28	15.05± 0.10	—
¹⁴⁶ Nd	13.01	14.88	14.23	16.15	13.35	15.23	13.34	15.47	14.80± 0.10	—
¹⁴⁸ Nd	12.55	14.91	13.75	16.25	13.06	15.35	13.09	15.57	14.70± 0.15	—
¹⁵⁰ Nd	11.87	15.18	13.12	16.55	12.27	15.68	12.44	15.91	12.30± 0.15	16.00± 0.15
¹⁵² Nd	11.80	15.18	12.87	16.60	12.20	15.73	12.34	15.93	—	—
¹⁵⁴ Nd	11.66	15.01	12.75	16.53	12.09	15.64	12.22	15.81	—	—
¹⁵⁶ Nd	11.55	14.88	12.64	16.44	11.98	15.58	12.10	15.75	—	—
¹⁵⁸ Nd	11.43	14.77	12.54	16.32	11.89	15.46	12.02	15.64	—	—
¹⁶⁰ Nd	11.29	14.63	12.45	16.15	11.82	15.35	11.93	15.51	—	—

all Skyrme forces that the GDR splitting ΔE decreases firstly when N increases from N=64 until N=82 (magic Number) which corresponds to spherical nucleus ¹⁴²Nd and then increases again until N=100 which correspond to well deformed nucleus ¹⁶⁰Nd. It confirms that the deformation structure of the nuclei is responsible to the division peak in the deformed nuclei.

Since the GDR splitting is caused by the deformation, it is possible to relate the nuclear deformation with the distance ΔE between two peaks of GDR spectra. In Fig. 13 is plotted the ratio $\Delta E/\bar{E}_m$ for ^{124–160}Nd isotopes as a function of the quadrupole deformation parameter β_2 . For the four Skyrme forces, we see that there is an approximate linear relation between $\Delta E/\bar{E}_m$ and β_2 of the general form

$$\Delta E/\bar{E}_m = a.\beta_2 + b, \quad (16)$$

where a and b are parameters depend on the Skyrme force, but they have very close values. For example, in the case of SVbas: $a \simeq 0.691$ and $b \simeq 0.006$ and in the case of SLy6: $a \simeq 0.676$ and $b \simeq 0.005$. The relation (16) was already studied in Refs. [13,14,54].

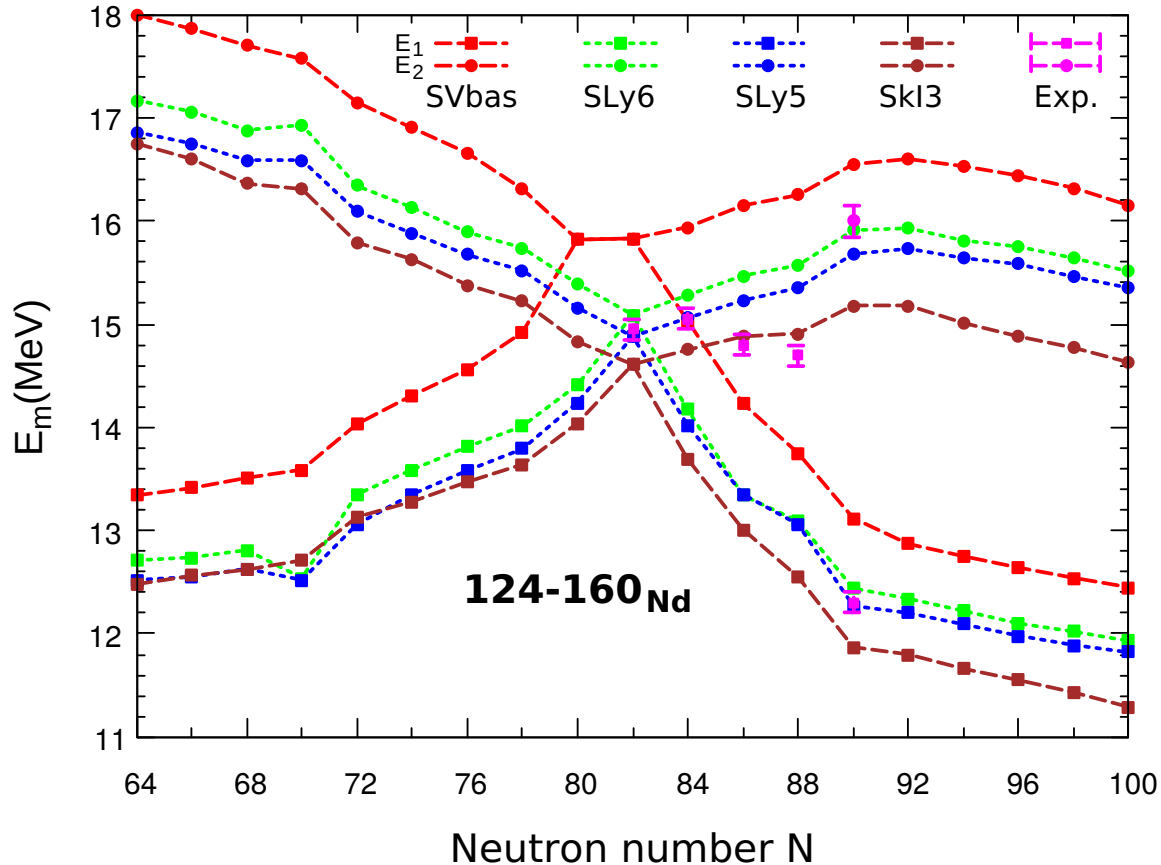


Figure 10: The peak position E_m of GDRs along major axis (circle symbol) and minor axis (square symbol) in Nd isotopes.

5. Conclusion

We have studied the GDR in $^{124-160}\text{Nd}$ isotopes with TDHF method based on Skyrme functional, using SKY3D code [22]. This study covers 19 isotopes of Nd with four Skyrme forces SkI3, SVbas, SLy5 and SLy6. Deformation parameters (β , γ), resonance energy centroids (E_m , E_m^1 , E_m^2) have been calculated for $^{124-160}\text{Nd}$ isotopes. The even isotopes of Nd from $A=124$ to $A=130$ and from $A=144$ to $A=160$ are of prolate shape with $\gamma \simeq 0^\circ$. The nuclei ^{132}Nd , ^{134}Nd , ^{136}Nd and ^{138}Nd are weakly triaxial. The nucleus ^{142}Nd is of a spherical shape with $\beta \simeq 0$. The dipole moment $D_m(t)$ of GDR calculation showed that oscillation frequency along the major axis is lower than that along the minor axis of the deformed axially nuclei as ^{150}Nd , and is the same along the three axes in spherical nuclei as ^{142}Nd .

In addition, the GDR strength calculated is compared with the experimental data. The results showed that TDHF method can reproduce the shape of the GDR spectra with a small shift depending on the used Skyrme force. The Skyrme forces SLy6, SLy5 and SVbas reproduce well the experimental data compared to SkI3, with a slight advantage for SLy6.

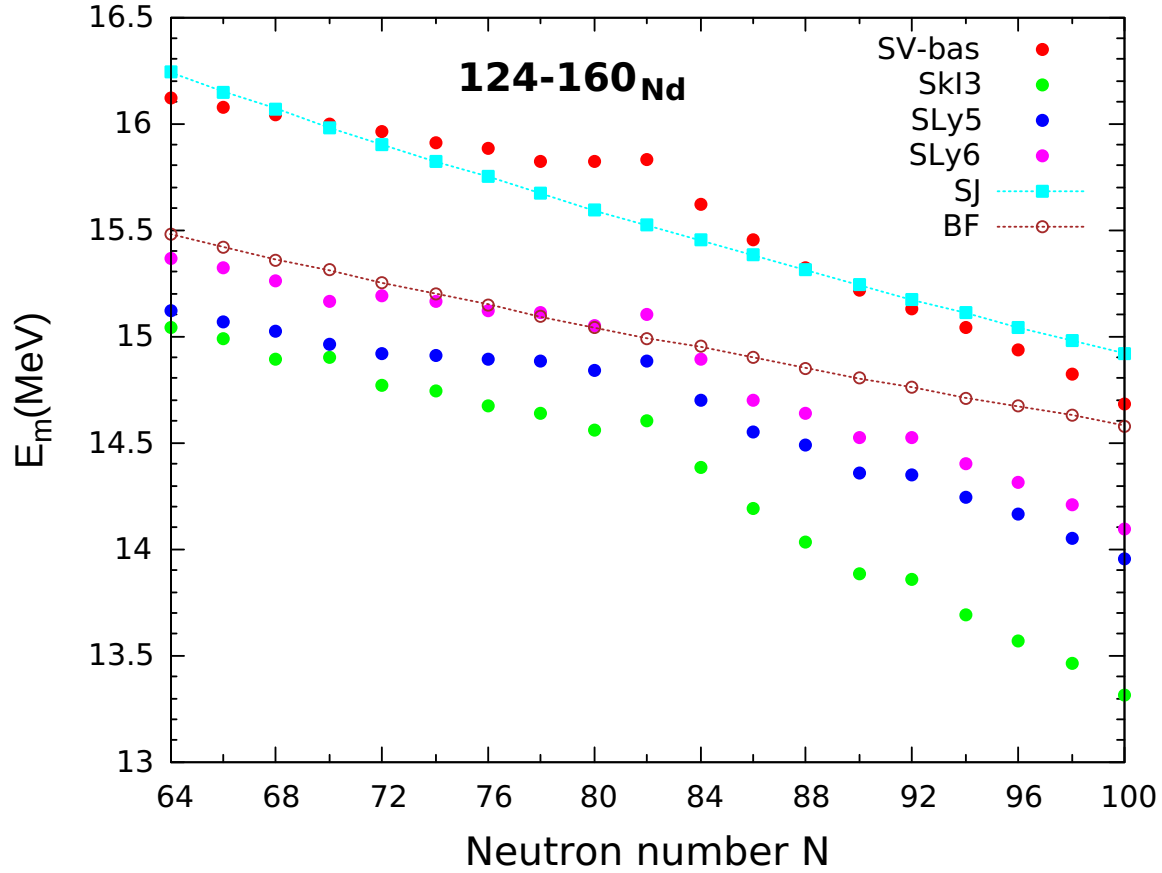


Figure 11: The resonance energies E_m in Nd isotopes compared with the estimates SJ((14)) and BF(15).

Resonance energies and GDR splitting ΔE are well described. We have found a correlation between the ratio $\Delta E/\bar{E}$ and the deformation parameter β_2 . For the isotopic chain of Nd, $\Delta E/\bar{E}_m \simeq 0.670\beta_2 + 0.005$. It confirms that the splitting of GDR spectra is proportional to the deformation of the nucleus.

Acknowledgement

Discussion with Prof. Paul Stevenson from university of serrey, Prof. Paul-Gerhard Reinhard and Prof. Sait Umar from Vanderbilt University is acknowledged.

References

- [1] Goldhaber M and Teller E 1948 *Physical Review* **74** 1046 URL <https://link.aps.org/doi/10.1103/PhysRev.74.1046>
- [2] Speth J and van der Woude A 1981 *Reports on Progress in Physics* **44** 719
- [3] Berman B L and Fultz S C 1975 *Rev. Mod. Phys.* **47**(3) 713–761 URL <https://link.aps.org/doi/10.1103/RevModPhys.47.713>
- [4] Carlos P, Beil H, Bergere R, Lepretre A and Veyssiere A 1971 *Nuclear Physics A* **172** 437–448

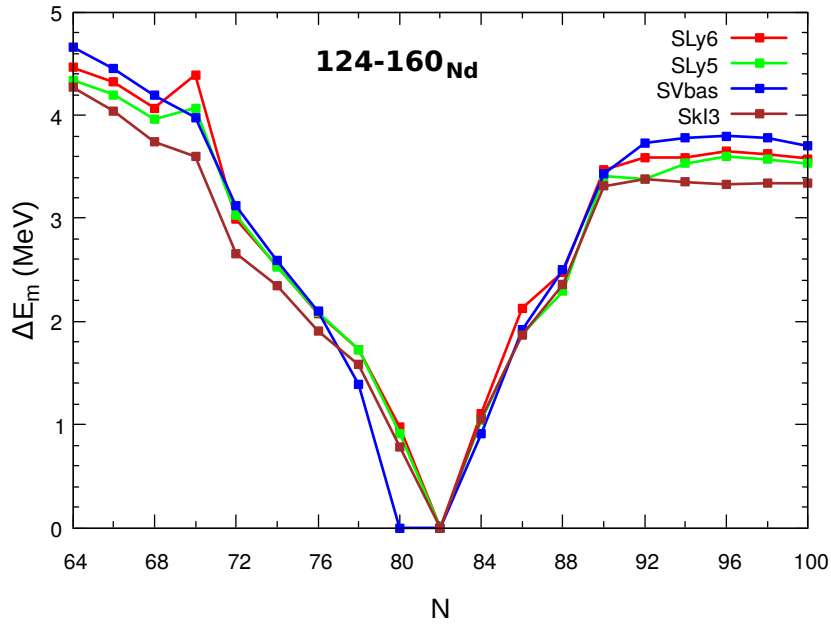


Figure 12: The GDR splitting as a function of the number of neutrons N in the case of $^{124-160}\text{Nd}$ isotopes calculated with SLy6, SLy5, SVbas and SkI3.

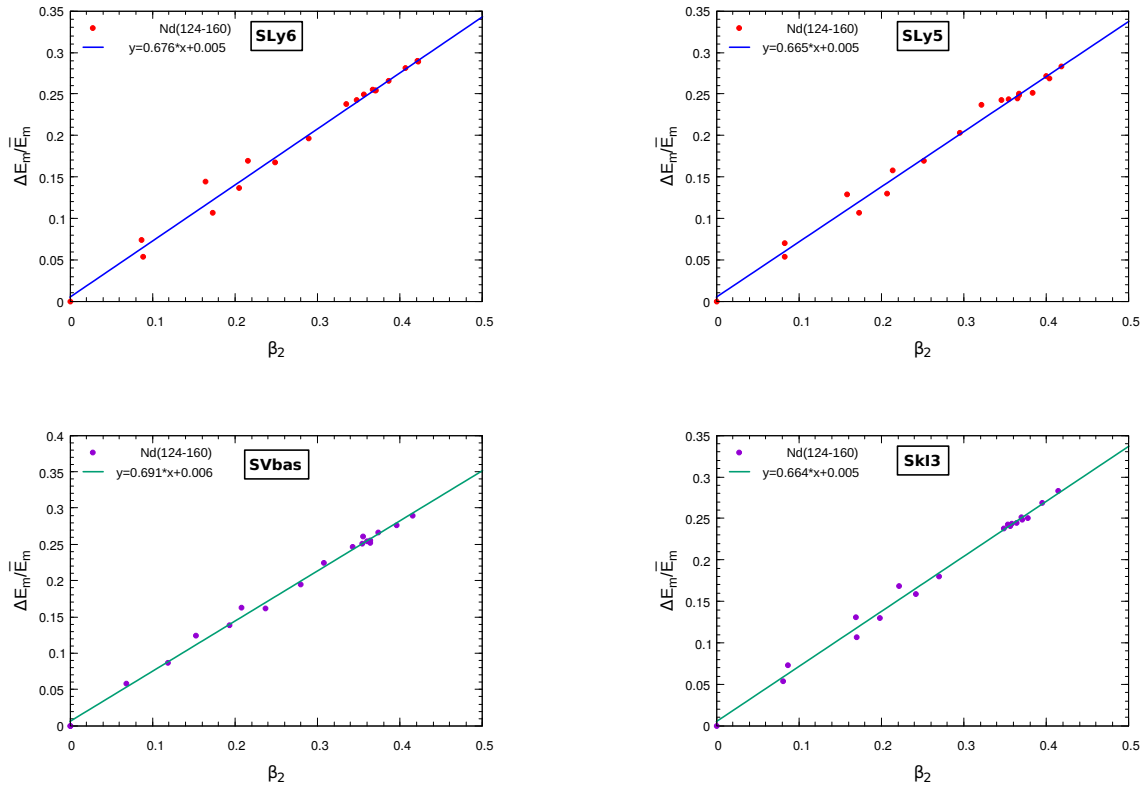


Figure 13: The correlation between the deformation parameter β_2 and the ratio $\Delta E/\bar{E}$. circles denote the data in the Nd isotopes and lines are the fitting results.

- [5] Donaldson L, Bertulani C, Carter J and al 2018 Physics Letters B **776** 133 – 138 ISSN 0370-2693 URL <http://www.sciencedirect.com/science/article/pii/S0370269317309176>
- [6] Goeke K and Speth J 1982 Annual Review of Nuclear and Particle Science **32** 65–115
- [7] Maruhn J A, Reinhard P G, Stevenson P D, Stone J R and Strayer M R 2005 Phys. Rev. C **71**(6) 064328 URL <https://link.aps.org/doi/10.1103/PhysRevC.71.064328>
- [8] Kleinig W, Nesterenko V O, Kvasil J, Reinhard P G and Vesely P 2008 Phys. Rev. C **78**(4) 044313 URL <https://link.aps.org/doi/10.1103/PhysRevC.78.044313>
- [9] Yoshida K and Nakatsukasa T 2011 Phys. Rev. C **83**(2) 021304 URL <https://link.aps.org/doi/10.1103/PhysRevC.83.021304>
- [10] Danos M 1958 Nuclear Physics **5** 23–32
- [11] Fracasso S, Suckling E B and Stevenson P 2012 Physical Review C **86** 044303
- [12] Nesterenko V, Kleinig W, Kvasil J, Vesely P and Reinhard P G 2007 International Journal of Modern Physics E **16** 624–633 URL <https://doi.org/10.1142/S0218301307006071>
- [13] Arteaga D P n, Khan E and Ring P 2009 Phys. Rev. C **79**(3) 034311 URL <https://link.aps.org/doi/10.1103/PhysRevC.79.034311>
- [14] Wang S S, Ma Y G, Cao X G, He W B, Kong H Y and Ma C W 2017 Phys. Rev. C **95**(5) 054615 URL <https://link.aps.org/doi/10.1103/PhysRevC.95.054615>
- [15] Masur V M and Mel'nikova L M 2006 Physics of Particles and Nuclei **37** 923–940 ISSN 1531-8559 URL <https://doi.org/10.1134/S1063779606060050>
- [16] Ramakrishnan E, Baumann T and al 1996 Physical review letters **76** 2025
- [17] Gundlach J, Snover K, Behr J and al 1990 Physical review letters **65** 2523
- [18] Blocki J and Flocard H 1979 Physics Letters B **85** 163–166 URL [https://doi.org/10.1016/0370-2693\(79\)90568-9](https://doi.org/10.1016/0370-2693(79)90568-9)
- [19] Chomaz P, Van Giai N and Stringari S 1987 Physics Letters B **189** 375–380 URL [https://doi.org/10.1016/0370-2693\(87\)90643-5](https://doi.org/10.1016/0370-2693(87)90643-5)
- [20] Maruhn J A, Reinhard P G, Stevenson P D and Strayer M R 2006 Phys. Rev. C **74**(2) 027601 URL <https://link.aps.org/doi/10.1103/PhysRevC.74.027601>
- [21] D Stevenson P, R Strayer M, Stone J and Newton W 2003 International Journal of Modern Physics E **13** 181–185
- [22] Schuetrumpf B, Reinhard P G, Stevenson P, Umar A and Maruhn J 2018 Computer Physics Communications **229** 211 – 213 ISSN 0010-4655 URL <http://www.sciencedirect.com/science/article/pii/S0010465518300845>
- [23] Reinhard P G and Flocard H 1995 Nuclear Physics A **584** 467 – 488 ISSN 0375-9474 URL <http://www.sciencedirect.com/science/article/pii/037594749400770N>
- [24] Chabanat E, Bonche P, Haensel P, Meyer J and Schaeffer R 1998 Nuclear Physics A **635** 231 – 256 ISSN 0375-9474 URL <http://www.sciencedirect.com/science/article/pii/S0375947498001808>
- [25] Negele J W 1982 Reviews of Modern Physics **54** 913
- [26] Dirac P A M 1930 Mathematical Proceedings of the Cambridge Philosophical Society **26** 376
- [27] Reinhard P G, Guo L and Maruhn J 2007 The European Physical Journal A **32** 19–23
- [28] Simenel C and Umar A 2018 Progress in Particle and Nuclear Physics **103** 19 – 66 ISSN 0146-6410 URL <http://www.sciencedirect.com/science/article/pii/S0146641018300693>
- [29] Engel Y, Brink D, Goeke K, Krieger S and Vautherin D 1975 Nuclear Physics A **249** 215 – 238 ISSN 0375-9474 URL <http://www.sciencedirect.com/science/article/pii/0375947475901840>
- [30] Kerman A and Koonin S 1976 Annals of Physics **100** 332 – 358 ISSN 0003-4916 URL <http://www.sciencedirect.com/science/article/pii/0003491676900658>
- [31] Koonin S E, Davies K T R, Maruhn-Rezwani V, Feldmeier H, Krieger S J and Negele J W 1977 Phys. Rev. C **15**(4) 1359–1374 URL <https://link.aps.org/doi/10.1103/PhysRevC.15.1359>
- [32] Simenel C 2012 Eur. Phys. J. A **48** 152 (*Preprint* 1209.3375)
- [33] Flocard H, Koonin S E and Weiss M S 1978 Phys. Rev. C **17**(5) 1682–1699 URL <https://link.aps.org/doi/10.1103/PhysRevC.17.1682>

- [34] Bonche P, Koonin S and Negele J W 1976 Phys. Rev. C **13**(3) 1226–1258 URL <https://link.aps.org/doi/10.1103/PhysRevC.13.1226>
- [35] Skyrme T 1958 Nuclear Physics **9** 615 – 634 ISSN 0029-5582 URL <http://www.sciencedirect.com/science/article/pii/0029558258903456>
- [36] Klüpfel P, Reinhard P G, Bürvenich T J and Maruhn J A 2009 Phys. Rev. C **79**(3) 034310 URL <https://link.aps.org/doi/10.1103/PhysRevC.79.034310>
- [37] Simenel C and Chomaz P 2009 Phys. Rev. C **80**(6) 064309 URL <https://link.aps.org/doi/10.1103/PhysRevC.80.064309>
- [38] Broomfield J M A and Stevenson P D 2008 Journal of Physics G: Nuclear and Particle Physics **35** 095102 URL <https://doi.org/10.1088/0954-3899/35/9/095102>
- [39] Ring P and Schuck P 1980 The nuclear many-body problem (New York: Springer-Verlag)
- [40] Reinhard P G, Stevenson P D, Almeded D, Maruhn J A and Strayer M R 2006 Phys. Rev. E **73**(3) 036709 URL <https://link.aps.org/doi/10.1103/PhysRevE.73.036709>
- [41] N Takigawa K W 2017 "Fundamentals of Nuclear Physics" (Tokyo: Springer Japan)
- [42] RAMAN S, NESTOR C and TIKKANEN P 2001 Atomic Data and Nuclear Data Tables **78** 1 – 128 ISSN 0092-640X URL <http://www.sciencedirect.com/science/article/pii/S0092640X01908587>
- [43] Delaroche J P, Girod M, Libert J, Goutte H, Hilaire S, Péru S, Pillet N and Bertsch G 2010 Physical Review C **81** 014303 URL <https://doi.org/10.1103/PhysRevC.81.014303>
- [44] Reinhard P G 2019 "private communication"
- [45] Xiang J, Li Z, Long W, Nikšić T and Vretenar D 2018 Physical Review C **98** 054308 URL <https://doi.org/10.1103/PhysRevC.98.054308>
- [46] Nesterenko V, Kleinig W, Kvasil J, Vesely P and Reinhard P G 2008 International Journal of Modern Physics E **17** 89–99
- [47] Oishi T, Kortelainen M and Hinohara N 2016 Phys. Rev. C **93**(3) 034329 URL <https://link.aps.org/doi/10.1103/PhysRevC.93.034329>
- [48] Nikšić T, Vretenar D and Ring P 2008 Phys. Rev. C **78**(3) 034318 URL <https://link.aps.org/doi/10.1103/PhysRevC.78.034318>
- [49] Nikšić T, Paar N, Vretenar D and Ring P 2014 Computer Physics Communications **185** 1808 – 1821 ISSN 0010-4655 URL <http://www.sciencedirect.com/science/article/pii/S0010465514000836>
- [50] Lalazissis G A, Nikšić T, Vretenar D and Ring P 2005 Phys. Rev. C **71**(2) 024312 URL <https://link.aps.org/doi/10.1103/PhysRevC.71.024312>
- [51] Roca-Maza X, Viñas X, Centelles M, Ring P and Schuck P 2011 Phys. Rev. C **84**(5) 054309 URL <https://link.aps.org/doi/10.1103/PhysRevC.84.054309>
- [52] Nikšić T, Vretenar D, Finelli P and Ring P 2002 Phys. Rev. C **66**(2) 024306 URL <https://link.aps.org/doi/10.1103/PhysRevC.66.024306>
- [53] Steinwedel H and Jensen J 1950 Z.Naturforsch 5A 413–420
- [54] Okamoto K 1958 Phys. Rev. **110**(1) 143–153 URL <https://link.aps.org/doi/10.1103/PhysRev.110.143>